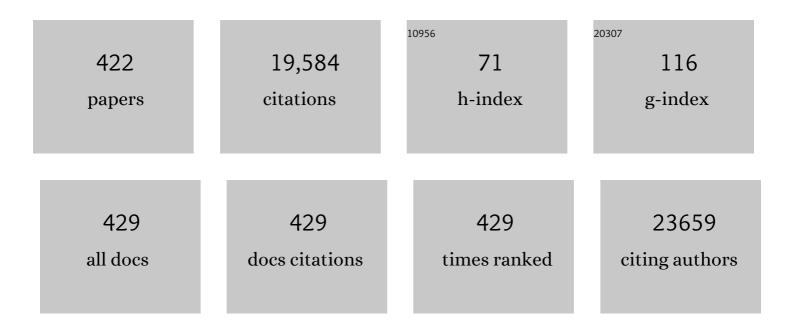
## Weitao Zheng

List of Publications by Year in descending order

Source: https://exaly.com/author-pdf/6715773/publications.pdf Version: 2024-02-01



#	Article	IF	CITATIONS
1	Light scattering and surface plasmons on small spherical particles. Light: Science and Applications, 2014, 3, e179-e179.	7.7	450
2	Polymerâ€Passivated Inorganic Cesium Lead Mixedâ€Halide Perovskites for Stable and Efficient Solar Cells with High Openâ€Circuit Voltage over 1.3 V. Advanced Materials, 2018, 30, 1705393.	11.1	401
3	Towards High‧afe Lithium Metal Anodes: Suppressing Lithium Dendrites via Tuning Surface Energy. Advanced Science, 2017, 4, 1600168.	5.6	399
4	Single-atom cobalt array bound to distorted 1T MoS2 with ensemble effect for hydrogen evolution catalysis. Nature Communications, 2019, 10, 5231.	5.8	371
5	Adsorption and Diffusion of Li on Pristine and Defective Graphene. ACS Applied Materials & Interfaces, 2012, 4, 2432-2438.	4.0	363
6	Trifluoroacetate induced small-grained CsPbBr3 perovskite films result in efficient and stable light-emitting devices. Nature Communications, 2019, 10, 665.	5.8	350
7	Formation Mechanism of Î2-Phase in PVDF/CNT Composite Prepared by the Sonication Method. Macromolecules, 2009, 42, 8870-8874.	2.2	300
8	Rational Design of Fe–N/C Hybrid for Enhanced Nitrogen Reduction Electrocatalysis under Ambient Conditions in Aqueous Solution. ACS Catalysis, 2019, 9, 336-344.	5.5	278
9	Smoothing the energy transfer pathway in quasi-2D perovskite films using methanesulfonate leads to highly efficient light-emitting devices. Nature Communications, 2021, 12, 1246.	5.8	274
10	Global Structural Optimization of Tungsten Borides. Physical Review Letters, 2013, 110, 136403.	2.9	253
11	Atomic-level energy storage mechanism of cobalt hydroxide electrode for pseudocapacitors. Nature Communications, 2017, 8, 15194.	5.8	250
12	Waterâ€Assisted Size and Shape Control of CsPbBr <sub>3</sub> Perovskite Nanocrystals. Angewandte Chemie - International Edition, 2018, 57, 3337-3342.	7.2	223
13	Inorganic CsPbI <sub>2</sub> Br Perovskite Solar Cells: The Progress and Perspective. Solar Rrl, 2019, 3, 1800239.	3.1	217
14	Pressure Effects on Structure and Optical Properties in Cesium Lead Bromide Perovskite Nanocrystals. Journal of the American Chemical Society, 2017, 139, 10087-10094.	6.6	214
15	Constructing 2D graphitic carbon nitride nanosheets/layered MoS2/graphene ternary nanojunction with enhanced photocatalytic activity. Applied Catalysis B: Environmental, 2018, 225, 468-476.	10.8	208
16	Spontaneous Silver Doping and Surface Passivation of CsPbI <sub>3</sub> Perovskite Active Layer Enable Light-Emitting Devices with an External Quantum Efficiency of 11.2%. ACS Energy Letters, 2018, 3, 1571-1577.	8.8	205
17	Inverted Design for Highâ€Performance Supercapacitor Via Co(OH) <sub>2</sub> â€Derived Highly Oriented MOF Electrodes. Advanced Energy Materials, 2018, 8, 1702294.	10.2	205
18	Adsorption of Single Li and the Formation of Small Li Clusters on Graphene for the Anode of Lithium-Ion Batteries. ACS Applied Materials & Interfaces, 2013, 5, 7793-7797.	4.0	190

#	Article	IF	CITATIONS
19	N, S co-doped graphene quantum dots-graphene-TiO2 nanotubes composite with enhanced photocatalytic activity. Journal of Alloys and Compounds, 2017, 691, 369-377.	2.8	187
20	A Review for Aqueous Electrochemical Supercapacitors. Frontiers in Energy Research, 2015, 3, .	1.2	174
21	Reactive magnetron sputter deposited CNx: Effects of N2 pressure and growth temperature on film composition, bonding, and microstructure. Journal of Vacuum Science and Technology A: Vacuum, Surfaces and Films, 1996, 14, 2696-2701.	0.9	172
22	Density Functional Theory Calculations for the Quantum Capacitance Performance of Graphene-Based Electrode Material. Journal of Physical Chemistry C, 2015, 119, 6464-6470.	1.5	166
23	Saturation magnetization of ferromagnetic and ferrimagnetic nanocrystals at room temperature. Journal Physics D: Applied Physics, 2007, 40, 320-325.	1.3	164
24	Synthesis of Co(OH)2/graphene/Ni foam nano-electrodes with excellent pseudocapacitive behavior and high cycling stability for supercapacitors. International Journal of Hydrogen Energy, 2012, 37, 11846-11852.	3.8	163
25	Ultrahigh capacitive performance from both Co(OH)2/graphene electrode and K3Fe(CN)6 electrolyte. Scientific Reports, 2013, 3, 2986.	1.6	158
26	Hydrogen Stabilized RhPdH 2D Bimetallene Nanosheets for Efficient Alkaline Hydrogen Evolution. Journal of the American Chemical Society, 2020, 142, 3645-3651.	6.6	152
27	PbS Capped CsPbI <sub>3</sub> Nanocrystals for Efficient and Stable Light-Emitting Devices Using <i>p</i> – <i>i</i> – <i>n</i> Structures. ACS Central Science, 2018, 4, 1352-1359.	5.3	141
28	Well-dispersed palladium nanoparticles on graphene oxide as a non-enzymatic glucose sensor. RSC Advances, 2012, 2, 6245.	1.7	138
29	Reduced graphene oxide/CdS for efficiently photocatalystic degradation of methylene blue. Journal of Alloys and Compounds, 2012, 524, 5-12.	2.8	136
30	Hydrogen-bond relaxation dynamics: Resolving mysteries of water ice. Coordination Chemistry Reviews, 2015, 285, 109-165.	9.5	136
31	Recent progress of TMD nanomaterials: phase transitions and applications. Nanoscale, 2020, 12, 1247-1268.	2.8	132
32	Highly Carbon-Doped TiO <sub>2</sub> Derived from MXene Boosting the Photocatalytic Hydrogen Evolution. ACS Sustainable Chemistry and Engineering, 2018, 6, 13480-13486.	3.2	130
33	Decoration of the inert basal plane of defect-rich MoS <sub>2</sub> with Pd atoms for achieving Pt-similar HER activity. Journal of Materials Chemistry A, 2016, 4, 4025-4031.	5.2	122
34	Coordination-Resolved Electron Spectrometrics. Chemical Reviews, 2015, 115, 6746-6810.	23.0	121
35	Development of microstructure CO sensor based on hierarchically porous ZnO nanosheet thin films. Sensors and Actuators B: Chemical, 2012, 173, 897-902.	4.0	120
36	Density and Phonon-Stiffness Anomalies of Water and Ice in the Full Temperature Range. Journal of Physical Chemistry Letters, 2013, 4, 3238-3244.	2.1	116

#	Article	IF	CITATIONS
37	(EMIm) <sup>+</sup> (PF <sub>6</sub> ) <sup>â^'</sup> Ionic Liquid Unlocks Optimum Energy/Power Density for Architecture of Nanocarbonâ€Based Dualâ€Ion Battery. Advanced Energy Materials, 2016, 6, 1601378.	10.2	116
38	Density, Elasticity, and Stability Anomalies of Water Molecules with Fewer than Four Neighbors. Journal of Physical Chemistry Letters, 2013, 4, 2565-2570.	2.1	115
39	Revealing the Intrinsic Peroxidase-Like Catalytic Mechanism of Heterogeneous Single-Atom Co–MoS2. Nano-Micro Letters, 2019, 11, 102.	14.4	114
40	One-Step Synthesis of a Self-Supported Copper Phosphide Nanobush for Overall Water Splitting. ACS Omega, 2016, 1, 1367-1373.	1.6	113
41	NiAl(110)â^•Cr(110)interface: A density functional theory study. Physical Review B, 2006, 73, .	1.1	112
42	Experimental and modelling investigations on strain rate sensitivity of an electrodeposited 20 nm grain sized Ni. Journal Physics D: Applied Physics, 2007, 40, 7440-7446.	1.3	110
43	Single Atom Excels as the Smallest Functional Material. Advanced Functional Materials, 2016, 26, 2988-2993.	7.8	110
44	Tent-pitching-inspired high-valence period 3-cation pre-intercalation excels for anode of 2D titanium carbide (MXene) with high Li storage capacity. Energy Storage Materials, 2019, 16, 163-168.	9.5	110
45	A novel low compressible and superhard carbon nitride: Body-centered tetragonal CN2. Physical Chemistry Chemical Physics, 2012, 14, 13081.	1.3	108
46	Anomalous Stress Response of Ultrahard <mml:math xmlns:mml="http://www.w3.org/1998/Math/MathML" display="inline"&gt;<mml:mrow><mml:msub><mml:mrow><mml:mi>WB</mml:mi></mml:mrow><mml:mrow><m Physical Review Letters, 2015, 115, 185502.</m </mml:mrow></mml:msub></mml:mrow></mml:math 	nl:mi>n <td>107 nml:mi&gt;</td>	107 nml:mi>
47	Favorable Energy Band Alignment of TiO <sub>2</sub> Anatase/Rutile Heterophase Homojunctions Yields Photocatalytic Hydrogen Evolution with Quantum Efficiency Exceeding 45.6%. Advanced Energy Materials, 2022, 12, .	10.2	106
48	Photo-assisted preparation and patterning of large-area reduced graphene oxide–TiO2 conductive thin film. Chemical Communications, 2010, 46, 3499.	2.2	105
49	Amorphous carbon enriched with pyridinic nitrogen as an efficient metal-free electrocatalyst for oxygen reduction reaction. Chemical Communications, 2014, 50, 557-559.	2.2	105
50	Controlling phase transition for single-layer MTe <sub>2</sub> (M = Mo and W): modulation of the potential barrier under strain. Physical Chemistry Chemical Physics, 2016, 18, 4086-4094.	1.3	105
51	Iridium-Triggered Phase Transition of MoS <sub>2</sub> Nanosheets Boosts Overall Water Splitting in Alkaline Media. ACS Energy Letters, 2019, 4, 368-374.	8.8	105
52	A semiconductor-electrochemistry model for design of high-rate Li ion battery. Journal of Energy Chemistry, 2020, 41, 100-106.	7.1	103
53	Size and interface effects on ferromagnetic and antiferromagnetic transition temperatures. Physical Review B, 2006, 73, .	1.1	102
54	Lattice -Mismatch-Induced Ultrastable 1T-Phase MoS <sub>2</sub> –Pd/Au for Plasmon-Enhanced Hydrogen Evolution. Nano Letters, 2019, 19, 2758-2764.	4.5	98

#	Article	IF	CITATIONS
55	Electronic fitness function for screening semiconductors as thermoelectric materials. Physical Review Materials, 2017, 1, .	0.9	98
56	2D titanium carbide (MXene) electrodes with lower-F surface for high performance lithium-ion batteries. Journal of Energy Chemistry, 2019, 31, 148-153.	7.1	97
57	Controlled Synthesis of Hollow Cu <sub>2â€x</sub> Te Nanocrystals Based on the Kirkendall Effect and Their Enhanced CO Gasâ€5ensing Properties. Small, 2013, 9, 793-799.	5.2	94
58	Enhanced ammonia sensing performances of Pd-sensitized flowerlike ZnO nanostructure. Sensors and Actuators B: Chemical, 2011, 156, 395-400.	4.0	92
59	Shape-dependent catalytic activity of oxygen reduction reaction (ORR) on silver nanodecahedra and nanocubes. Journal of Power Sources, 2014, 269, 152-157.	4.0	89
60	The Electronic Properties of Single-Layer and Multilayer MoS <sub>2</sub> under High Pressure. Journal of Physical Chemistry C, 2015, 119, 10189-10196.	1.5	89
61	Ni(OH)2 nanoflakes electrodeposited on Ni foam-supported vertically oriented graphene nanosheets for application in asymmetric supercapacitors. Materials Research Bulletin, 2014, 52, 89-95.	2.7	87
62	Nitrogen/Boron Doping Position Dependence of the Electronic Properties of a Triangular Graphene. ACS Nano, 2010, 4, 7619-7629.	7.3	86
63	Nanoporous Sulfur-Doped Copper Oxide (Cu <sub>2</sub> O <sub><i>x</i></sub> S <sub>1–<i>x</i></sub> ) for Overall Water Splitting. ACS Applied Materials & Interfaces, 2018, 10, 745-752.	4.0	83
64	First-principles study of the surface energy and work function of III-V semiconductor compounds. Physical Review B, 2007, 75, .	1.1	82
65	Surface plasmon resonance technique for directly probing the interaction of DNA and graphene oxide and ultra-sensitive biosensing. Biosensors and Bioelectronics, 2014, 58, 374-379.	5.3	81
66	The hidden force opposing ice compression. Chemical Science, 2012, 3, 1455.	3.7	80
67	Size, separation, structural order and mass density of molecules packing in water and ice. Scientific Reports, 2013, 3, 3005.	1.6	76
68	One-step synthesis of band-tunable N, S co-doped commercial TiO <sub>2</sub> /graphene quantum dots composites with enhanced photocatalytic activity. RSC Advances, 2017, 7, 23319-23327.	1.7	76
69	Field emission properties of N-doped capped single-walled carbon nanotubes: A first-principles density-functional study. Journal of Chemical Physics, 2007, 126, 164702.	1.2	74
70	Valence Band Splitting on Multilayer MoS <sub>2</sub> : Mixing of Spin–Orbit Coupling and Interlayer Coupling. Journal of Physical Chemistry Letters, 2016, 7, 2175-2181.	2.1	73
71	Toughness enhancement and tribochemistry of the Nb-Ag-N films actuated by solute Ag. Acta Materialia, 2017, 137, 1-11.	3.8	73
72	Vertically co-oriented two dimensional metal-organic frameworks for packaging enhanced supercapacitive performance. Communications Chemistry, 2018, 1, .	2.0	73

#	Article	IF	CITATIONS
73	Improving the Quantum Capacitance of Graphene-Based Supercapacitors by the Doping and Co-Doping: First-Principles Calculations. ACS Omega, 2019, 4, 13209-13217.	1.6	73
74	Effects of doping nitrogen atoms on the structure and electronic properties of zigzag single-walled carbon nanotubes through first-principles calculations. Nanotechnology, 2007, 18, 165702.	1.3	72
75	Oxygen Vacancies Boost δ-Bi <sub>2</sub> O <sub>3</sub> as a High-Performance Electrode for Rechargeable Aqueous Batteries. ACS Applied Materials & Interfaces, 2019, 11, 2103-2111.	4.0	72
76	Energy Level Modification with Carbon Dot Interlayers Enables Efficient Perovskite Solar Cells and Quantum Dot Based Lightâ€Emitting Diodes. Advanced Functional Materials, 2020, 30, 1910530.	7.8	72
77	Hydrothermal reduction of graphene oxide; effect on surfaceâ€enhanced Raman scattering. Journal of Raman Spectroscopy, 2017, 48, 97-103.	1.2	70
78	Synthesis of ultrathin wrinkle-free PdCu alloy nanosheets for modulating d-band electrons for efficient methanol oxidation. Journal of Materials Chemistry A, 2018, 6, 8531-8536.	5.2	70
79	Thermally Activated Upconversion Nearâ€Infrared Photoluminescence from Carbon Dots Synthesized via Microwave Assisted Exfoliation. Small, 2019, 15, e1905050.	5.2	70
80	Ar plasma treatment on few layer graphene sheets for enhancing their field emission properties. Journal Physics D: Applied Physics, 2010, 43, 055302.	1.3	69
81	Interaction between graphene and the surface of SiO <sub>2</sub> . Journal of Physics Condensed Matter, 2012, 24, 305004.	0.7	69
82	Raman spectroscopic determination of the length, strength, compressibility, Debye temperature, elasticity, and force constant of the C–C bond in graphene. Nanoscale, 2012, 4, 502-510.	2.8	69
83	High-Pressure Phase Stability and Superconductivity of Pnictogen Hydrides and Chemical Trends for Compressed Hydrides. Chemistry of Materials, 2016, 28, 1746-1755.	3.2	68
84	Engineering of Transition Metal Sulfide Nanostructures as Efficient Electrodes for High-Performance Supercapacitors. ACS Applied Energy Materials, 2022, 5, 6481-6498.	2.5	68
85	Coulomb Repulsion at the Nanometer-Sized Contact: A Force Driving Superhydrophobicity, Superfluidity, Superlubricity, and Supersolidity. Journal of Physical Chemistry C, 2009, 113, 20009-20019.	1.5	67
86	Interstitial Hydrogen Atom Modulation to Boost Hydrogen Evolution in Pd-Based Alloy Nanoparticles. ACS Nano, 2019, 13, 12987-12995.	7.3	67
87	Hydrogen-bond memory and water-skin supersolidity resolving the Mpemba paradox. Physical Chemistry Chemical Physics, 2014, 16, 22995-23002.	1.3	65
88	Highly active zigzag-like Pt-Zn alloy nanowires with high-index facets for alcohol electrooxidation. Nano Research, 2019, 12, 1173-1179.	5.8	65
89	Multidentate Ligand Polyethylenimine Enables Bright Color-Saturated Blue Light-Emitting Diodes Based on CsPbBr <sub>3</sub> Nanoplatelets. ACS Energy Letters, 2021, 6, 477-484.	8.8	65
90	Atomistic origin, temperature dependence, and responsibilities of surface energetics: An extended broken-bond rule. Physical Review B, 2007, 75, .	1.1	64

#	Article	IF	CITATIONS
91	Rapid and selective H2S detection of hierarchical ZnSnO3 nanocages. Sensors and Actuators B: Chemical, 2011, 159, 245-250.	4.0	63
92	Water's phase diagram: From the notion of thermodynamics to hydrogen-bond cooperativity. Progress in Solid State Chemistry, 2015, 43, 71-81.	3.9	63
93	Adsorption of Li on single-layer silicene for anodes of Li-ion batteries. Physical Chemistry Chemical Physics, 2018, 20, 8887-8896.	1.3	62
94	Synthesis of graphene on a polycrystalline Co film by radio-frequency plasma-enhanced chemical vapour deposition. Journal Physics D: Applied Physics, 2010, 43, 455402.	1.3	61
95	A common supersolid skin covering both water and ice. Physical Chemistry Chemical Physics, 2014, 16, 22987-22994.	1.3	61
96	1D alignment of ZnO@ZIF-8/67 nanorod arrays for visible-light-driven photoelectrochemical water splitting. Applied Surface Science, 2018, 448, 254-260.	3.1	60
97	Graphene oxide-Ag nanocomposite: In situ photochemical synthesis and application as a surface-enhanced Raman scattering substrate. Thin Solid Films, 2011, 520, 179-185.	0.8	59
98	Synthesis of double-shelled SnO <sub>2</sub> nano-polyhedra and their improved gas sensing properties. Nanoscale, 2015, 7, 3276-3284.	2.8	59
99	Bottom-up growth of homogeneous Moiré superlattices in bismuth oxychloride spiral nanosheets. Nature Communications, 2019, 10, 4472.	5.8	59
100	Electrodeposited Ni(OH)2 nanoflakes on graphite nanosheets prepared by plasma-enhanced chemical vapor deposition for supercapacitor electrode. New Journal of Chemistry, 2012, 36, 1902.	1.4	58
101	Highly Ordered Periodic Au/TiO <sub>2</sub> Hetero-Nanostructures for Plasmon-Induced Enhancement of the Activity and Stability for Ethanol Electro-oxidation. ACS Applied Materials & Interfaces, 2016, 8, 5273-5279.	4.0	58
102	Integrating Catalysis of Methane Decomposition and Electrocatalytic Hydrogen Evolution with Ni/CeO <sub>2</sub> for Improved Hydrogen Production Efficiency. ChemSusChem, 2019, 12, 1000-1010.	3.6	58
103	Synthesis of polyhedron hollow structure Cu2O and their gas-sensing properties. Sensors and Actuators B: Chemical, 2012, 171-172, 135-140.	4.0	56
104	Electrical conductivity of carbon nanotube/poly(vinylidene fluoride) composites prepared by high-speed mechanical mixing. Carbon, 2012, 50, 339-341.	5.4	56
105	Assembly of hierarchical ZnSnO3 hollow microspheres from ultra-thin nanorods and the enhanced ethanol-sensing performances. Sensors and Actuators B: Chemical, 2014, 190, 370-377.	4.0	56
106	A high-performance asymmetric supercapacitor based on Co(OH) 2 /graphene and activated carbon electrodes. Journal of Electroanalytical Chemistry, 2016, 782, 98-102.	1.9	56
107	Perovskite Quantum Dots with Atomic Crystal Shells for Light-Emitting Diodes with Low Efficiency Roll-Off. ACS Energy Letters, 2020, 5, 2927-2934.	8.8	55
108	Improving Photocatalytic Performance from Bi2WO6@MoS2/graphene Hybrids via Gradual Charge Transferred Pathway. Scientific Reports, 2017, 7, 3637.	1.6	53

#	Article	IF	CITATIONS
109	Stress development during deposition of CNx thin films. Applied Physics Letters, 1998, 72, 2532-2534.	1.5	52
110	Exploiting the trade-offs of electron transfer in MOF-derived single Zn/Co atomic couples for performance-enhanced zinc-air battery. Applied Catalysis B: Environmental, 2022, 316, 121591.	10.8	51
111	First-principles density-functional investigation of the effect of water on the field emission of carbon nanotubes. Nanotechnology, 2007, 18, 155707.	1.3	50
112	Porous single-crystalline palladium nanoflowers with enriched {100} facets for highly enhanced ethanol oxidation. Nanoscale, 2014, 6, 15090-15097.	2.8	50
113	Ionothermal synthesis and proton-conductive properties of NH <sub>2</sub> -MIL-53 MOF nanomaterials. CrystEngComm, 2016, 18, 525-528.	1.3	50
114	Synthesis and the improved sensing properties of hierarchical SnO2 hollow nanosheets with mesoporous and multilayered interiors. Sensors and Actuators B: Chemical, 2016, 222, 354-361.	4.0	49
115	Zipperâ€Inspired SEI Film for Remarkably Enhancing the Stability of Li Metal Anode via Nucleation Barriers Controlled Weaving of Lithium Pits. Advanced Energy Materials, 2018, 8, 1800650.	10.2	49
116	Modeling lattice expansion and cohesive energy of nanostructured materials. Applied Physics Letters, 2009, 95, .	1.5	48
117	Stable Bimetallene Hydride Boosts Anodic CO Tolerance of Fuel Cells. ACS Energy Letters, 2021, 6, 1912-1919.	8.8	48
118	Discriminative generation and hydrogen modulation of the Dirac-Fermi polarons at graphene edges and atomic vacancies. Carbon, 2011, 49, 3615-3621.	5.4	47
119	Electron Scattering and Electrical Conductance in Polycrystalline Metallic Films and Wires: Impact of Grain Boundary Scattering Related to Melting Point. ACS Nano, 2010, 4, 3781-3788.	7.3	46
120	Carbonâ€Based Dualâ€lon Battery with Enhanced Capacity and Cycling Stability. ChemElectroChem, 2018, 5, 3612-3618.	1.7	46
121	Modulation of Hydrogen Evolution Catalytic Activity of Basal Plane in Monolayer Platinum and Palladium Dichalcogenides. ACS Omega, 2018, 3, 10058-10065.	1.6	46
122	Layered Tl <sub>2</sub> O: a model thermoelectric material. Journal of Materials Chemistry C, 2019, 7, 5094-5103.	2.7	46
123	Shape Control of Metal Halide Perovskite Single Crystals: From Bulk to Nanoscale. Chemistry of Materials, 2020, 32, 7602-7617.	3.2	46
124	Engineering graphene/carbon nanotube hybrid for direct electron transfer of glucose oxidase and glucose biosensor. Journal of Applied Electrochemistry, 2012, 42, 875-881.	1.5	45
125	Cu-Doped Layered Double Hydroxide Constructs the Performance-Enhanced Supercapacitor Via Band Gap Reduction and Defect Triggering. ACS Applied Energy Materials, 2022, 5, 2192-2201.	2.5	45
126	Electrical conductivity of poly(vinylidene fluoride)/carbon nanotube composites with a spherical substructure. Carbon, 2009, 47, 2118-2120.	5.4	44

#	Article	IF	CITATIONS
127	Low-temperature synthesis of porous hollow structured Cu2O for photocatalytic activity and gas sensor application. RSC Advances, 2013, 3, 18651.	1.7	44
128	Realâ€space observation of strong metalâ€support interaction: stateâ€ofâ€theâ€art and what's the next. Journal of Microscopy, 2016, 262, 203-215.	0.8	44
129	Effects of substrate bias on the preferred orientation, phase transition and mechanical properties for NbN films grown by direct current reactive magnetron sputtering. Journal of Applied Physics, 2008, 104, .	1.1	43
130	A Switch of the Oxidation State of Graphene Oxide on a Surface Plasmon Resonance Chip. ACS Applied Materials & Interfaces, 2013, 5, 2096-2103.	4.0	43
131	Ultrathin nanorod-assembled SnO2 hollow cubes for high sensitive n-butanol detection. Sensors and Actuators B: Chemical, 2019, 283, 693-704.	4.0	43
132	MOFs fertilized transition-metallic single-atom electrocatalysts for highly-efficient oxygen reduction: Spreading the synthesis strategies and advanced identification. Journal of Energy Chemistry, 2022, 67, 391-422.	7.1	43
133	Dependence of the blocking temperature in exchange biased ferromagnetic/antiferromagnetic bilayers on the thickness of the antiferromagnetic layer. Nanotechnology, 2007, 18, 155701.	1.3	42
134	Raman spectroscopy determination of the Debye temperature and atomic cohesive energy of CdS, CdSe, Bi2Se3, and Sb2Te3 nanostructures. Journal of Applied Physics, 2012, 112, .	1.1	42
135	Perspective: <i>n</i> -type oxide thermoelectrics via visual search strategies. APL Materials, 2016, 4, .	2.2	42
136	Plasmonic-induced inhibition and enhancement of the electrocatalytic activity of Pd-Au hetero-nanoraspberries for ethanol oxidation. Journal of Power Sources, 2016, 316, 29-36.	4.0	42
137	Adsorption and Formation of Small Na Clusters on Pristine and Double-Vacancy Graphene for Anodes of Na-Ion Batteries. ACS Applied Materials & amp; Interfaces, 2017, 9, 17076-17084.	4.0	42
138	Pd-loaded SnO2 ultrathin nanorod-assembled hollow microspheres with the significant improvement for toluene detection. Sensors and Actuators B: Chemical, 2017, 243, 465-474.	4.0	42
139	Crystallization of SiC and its effects on microstructure, hardness and toughness in TaC/SiC multilayer films. Ceramics International, 2018, 44, 613-621.	2.3	41
140	Amine-Terminated Carbon Dots Linking Hole Transport Layer and Vertically Oriented Quasi-2D Perovskites through Hydrogen Bonds Enable Efficient LEDs. ACS Nano, 2022, 16, 9679-9690.	7.3	41
141	Size distribution-controlled preparation of graphene oxide nanosheets with different C/O ratios. Materials Chemistry and Physics, 2013, 139, 8-11.	2.0	40
142	Thermoelectric properties of p-type cubic and rhombohedral GeTe. Journal of Applied Physics, 2018, 123,	1.1	40
143	Photovoltaic properties of graphene oxide sheets beaded with ZnO nanoparticles. Journal of Solid State Chemistry, 2011, 184, 881-887.	1.4	39
144	One-pot hydrothermal synthesis of mesoporous ZnxCd1â^'xS/reduced graphene oxide hybrid material and its enhanced photocatalytic activity. Dalton Transactions, 2014, 43, 12894.	1.6	39

#	Article	IF	CITATIONS
145	Controllable formation of multi-layered SnO <sub>2</sub> @Fe <sub>2</sub> O <sub>3</sub> sandwich cubes as a high-performance anode for Li-ion batteries. Nanoscale, 2017, 9, 17576-17584.	2.8	39
146	Quantum Capacitance of Silicene-Based Electrodes from First-Principles Calculations. Journal of Physical Chemistry C, 2018, 122, 1903-1912.	1.5	39
147	First principles study on 2H–1T′ transition in MoS <sub>2</sub> with copper. Physical Chemistry Chemical Physics, 2018, 20, 26986-26994.	1.3	39
148	<scp>MXene</scp> â€Based Quantum Dots Optimize Hydrogen Production via Spontaneous Evolution of Cl―to Oâ€Terminated Surface Groups. Energy and Environmental Materials, 2023, 6, .	7.3	39
149	Field emission enhancement of amorphous carbon films by nitrogen-implantation. Carbon, 2004, 42, 2309-2314.	5.4	38
150	Size and Structural Dependence of Cohesive Energy in Cu. Journal of Physical Chemistry C, 2008, 112, 18840-18845.	1.5	38
151	Pressure evolution of the potential barriers of phase transition of MoS <sub>2</sub> , MoSe <sub>2</sub> and MoTe <sub>2</sub> . Physical Chemistry Chemical Physics, 2016, 18, 12080-12085.	1.3	38
152	Enhanced tensile strength and thermal conductivity in copper diamond composites with B4C coating. Scientific Reports, 2017, 7, 10727.	1.6	38
153	New design for highly durable infrared-reflective coatings. Light: Science and Applications, 2018, 7, 17175-17175.	7.7	37
154	Waterâ€Assisted Size and Shape Control of CsPbBr <sub>3</sub> Perovskite Nanocrystals. Angewandte Chemie, 2018, 130, 3395-3400.	1.6	37
155	Increasing surface active Co2+ sites of MOF-derived Co3O4 for enhanced supercapacitive performance via NaBH4 reduction. Electrochimica Acta, 2018, 289, 319-323.	2.6	37
156	Crystallization behavior of poly(vinylidene fluoride)/montmorillonite nanocomposite. Polymer Engineering and Science, 2009, 49, 491-498.	1.5	36
157	The thermal and thermoelectric transport properties of SiSb, GeSb and SnSb monolayers. Journal of Materials Chemistry C, 2019, 7, 10652-10662.	2.7	36
158	Zone-selective photoelectronic measurements of the local bonding and electronic dynamics associated with the monolayer skin and point defects of graphite. RSC Advances, 2012, 2, 2377.	1.7	35
159	Architecture of Co-layered double hydroxide nanocages/graphene composite electrode with high electrochemical performance for supercapacitor. Journal of Energy Chemistry, 2018, 27, 507-512.	7.1	35
160	Exploiting Anti-T-shaped Graphene Architecture to Form Low Tortuosity, Sieve-like Interfaces for High-Performance Anodes for Li-Based Cells. ACS Central Science, 2018, 4, 81-88.	5.3	35
161	Adsorption of Na on silicene for potential anode for Na-ion batteries. Electrochimica Acta, 2019, 297, 497-503.	2.6	35
162	Multistep assembly of Au-loaded SnO2 hollow multilayered nanosheets for high-performance CO detection. Sensors and Actuators B: Chemical, 2016, 227, 362-372.	4.0	34

#	Article	IF	CITATIONS
163	Density-functional theory study of the microstructure, electronic structure, and optical properties of amorphous carbon. Physical Review B, 2007, 75, .	1.1	33
164	Stabilized monolayer 1T MoS2 embedded in CoOOH for highly efficient overall water splitting. Nanoscale, 2018, 10, 12330-12336.	2.8	33
165	Integrated MXene&CoFe <sub>2</sub> O <sub>4</sub> electrodes with multi-level interfacial architectures for synergistic lithium-ion storage. Nanoscale, 2019, 11, 15037-15042.	2.8	33
166	Synergistic Dual-Confinement Effect: Merit of Hollowly Metallic Co <sub>9</sub> S <sub>8</sub> in Packaging Enhancement of Electrochemical Performance of Li–S Batteries. ACS Applied Energy Materials, 2019, 2, 1428-1435.	2.5	33
167	Adsorption and Diffusion of Potassium on 2D SnC Sheets for Potential Highâ€Performance Anodic Applications of Potassiumâ€lon Batteries. ChemElectroChem, 2020, 7, 3832-3838.	1.7	33
168	Highly Conductive Amorphous Pentlandite Anchored with Ultrafine Platinum Nanoparticles for Efficient pHâ€Universal Hydrogen Evolution Reaction. Advanced Functional Materials, 2021, 31, 2105372.	7.8	33
169	Pseudocapacitive properties of cobalt hydroxide electrodeposited on Ni-foam-supported carbon nanomaterial. Materials Research Bulletin, 2013, 48, 3189-3195.	2.7	32
170	2DEGs at Perovskite Interfaces between KTaO3 or KNbO3 and Stannates. PLoS ONE, 2014, 9, e91423.	1.1	32
171	Multistep synthesis of non-spherical SnO 2 @SnO 2 yolk-shell cuboctahedra with nanoparticle-assembled porous structure for toluene detection. Sensors and Actuators B: Chemical, 2016, 231, 365-375.	4.0	32
172	Electron emission of carbon nitride films and mechanism for the nitrogen-lowered threshold in cold cathode. Journal of Applied Physics, 2003, 94, 2741-2745.	1.1	31
173	Effects of the chemical bonding on the optical and mechanical properties for germanium carbide films used as antireflection and protection coating of ZnS windows. Journal of Physics Condensed Matter, 2006, 18, 4231-4241.	0.7	31
174	Structural characteristics of poly(vinylidene fluoride)/clay nanocomposites. Materials Letters, 2008, 62, 747-750.	1.3	31
175	On the nature of point defect and its effect on electronic structure of rocksalt hafnium nitride films. Acta Materialia, 2014, 81, 315-325.	3.8	31
176	Identification and thermodynamic mechanism of the phase transition in hafnium nitride films. Acta Materialia, 2015, 90, 59-68.	3.8	31
177	Insight into graphene/hydroxide compositing mechanism for remarkably enhanced capacity. Journal of Power Sources, 2018, 399, 238-245.	4.0	31
178	Chemically Synthesized Carbon Nanorods with Dual Polarized Emission. ACS Nano, 2019, 13, 12024-12031.	7.3	31
179	Dehydrogenation of benzene on Pt(111) surface. Journal of Chemical Physics, 2008, 129, 164705.	1.2	30
180	Transformation from Silver Nanoprisms to Nanodecahedra in a Temperature-Controlled Photomediated Synthesis. Journal of Physical Chemistry C, 2012, 116, 24268-24273.	1.5	30

#	Article	IF	CITATIONS
181	Enhanced hydrogen sensing properties of graphene by introducing a mono-atom-vacancy. Physical Chemistry Chemical Physics, 2013, 15, 21016.	1.3	30
182	Kinetic effects in the photomediated synthesis of silver nanodecahedra and nanoprisms: combined effect of wavelength and temperature. Nanoscale, 2014, 6, 7295-7302.	2.8	30
183	Pressure-Induced Reversible Phase Transformation in Nanostructured Bi <sub>2</sub> Te <sub>3</sub> with Reduced Transition Pressure. Journal of Physical Chemistry C, 2015, 119, 3843-3848.	1.5	30
184	Cu4 Cluster Doped Monolayer MoS2 for CO Oxidation. Scientific Reports, 2015, 5, 11230.	1.6	30
185	Design of Hydrogen Storage Alloys/Nanoporous Metals Hybrid Electrodes for Nickel-Metal Hydride Batteries. Scientific Reports, 2016, 6, 27601.	1.6	30
186	Transition Metalâ€Nitrogenâ€Carbon Active Site for Oxygen Reduction Electrocatalysis: Beyond the Fascinations of TMâ€N <sub>4</sub> . ChemCatChem, 2019, 11, 655-668.	1.8	30
187	External Electric Field Modulated Electronic and Structural Properties of ã€^111〉 Si Nanowires. Journal of Physical Chemistry C, 2009, 113, 10384-10389.	1.5	29
188	First-Principles Calculations on the Emission Properties of Pristine and N-Doped Carbon Nanotubes. Journal of Physical Chemistry C, 2009, 113, 812-818.	1.5	29
189	Structural stability of single-layer MoS <sub>2</sub> under large strain. Journal of Physics Condensed Matter, 2015, 27, 105401.	0.7	29
190	Design of ternary alkaline-earth metal Sn( <scp>ii</scp> ) oxides with potential good p-type conductivity. Journal of Materials Chemistry C, 2016, 4, 4592-4599.	2.7	29
191	Adsorption of metal atoms on silicene: stability and quantum capacitance of silicene-based electrode materials. Physical Chemistry Chemical Physics, 2019, 21, 4276-4285.	1.3	29
192	Switching Optimally Balanced Fe–N Interaction Enables Extremely Stable Energy Storage. Energy and Environmental Materials, 2023, 6, .	7.3	29
193	Amorphous Carbon Interconnected Ultrafine CoMnP with Enhanced Co Electron Delocalization Yields Pt‣ike Activity for Alkaline Water Electrolysis. Advanced Functional Materials, 2022, 32, .	7.8	29
194	Water Nanodroplet Thermodynamics: Quasi-Solid Phase-Boundary Dispersivity. Journal of Physical Chemistry B, 2015, 119, 5265-5269.	1.2	28
195	Unifying miscellaneous performance criteria for a prototype supercapacitor via Co(OH) <sub>2</sub> active material and current collector interactions. Journal of Microscopy, 2017, 267, 34-48.	0.8	28
196	Mechanistic Origin of Enhanced CO Catalytic Oxidation over Co <sub>3</sub> O <sub>4</sub> /LaCoO <sub>3</sub> at Lower Temperature. ChemCatChem, 2017, 9, 3102-3106.	1.8	28
197	Bi-metal–organic frameworks type II heterostructures for enhanced photocatalytic styrene oxidation. Nanoscale, 2019, 11, 7554-7559.	2.8	28
198	Effects of nitrogen flow rate on the preferred orientation and phase transition for niobium nitride films grown by direct current reactive magnetron sputtering. Journal Physics D: Applied Physics, 2009, 42, 035304.	1.3	27

#	Article	IF	CITATIONS
199	Antiâ€Freezing Aqueous Electrolyte for Highâ€Performance Co(OH) <sub>2</sub> Supercapacitors at â~'30 °C. Energy Technology, 2018, 6, 605-612.	1.8	27
200	Optical coatings of durability based on transition metal nitrides. Thin Solid Films, 2019, 688, 137339.	0.8	27
201	Host–guest composite materials of LiCl/NaY with wide range of humidity sensitivity. Materials Letters, 2004, 58, 1535-1539.	1.3	26
202	One-pot photochemical synthesis of ultrathin Au nanocrystals on co-reduced graphene oxide and its application. Journal of Colloid and Interface Science, 2012, 383, 140-147.	5.0	26
203	Waveband-dependent photochemical processing of graphene oxide in fabricating reduced graphene oxide film and graphene oxide–Ag nanoparticles film. RSC Advances, 2013, 4, 2404-2408.	1.7	25
204	Negative effect of vacancies on cubic symmetry, hardness and conductivity in hafnium nitride films. Scripta Materialia, 2015, 108, 141-146.	2.6	25
205	Superconductivity in HfTe5 across weak to strong topological insulator transition induced via pressures. Scientific Reports, 2017, 7, 44367.	1.6	25
206	Compositional and structural modifications of amorphous carbon nitride films induced by thermal annealing. Journal Physics D: Applied Physics, 2003, 36, 2001-2005.	1.3	24
207	The AlN layer thickness dependent coherent epitaxial growth, stress and hardness in NbN/AlN nanostructured multilayer films. Surface and Coatings Technology, 2013, 235, 367-375.	2.2	24
208	A nanoflower shaped gold-palladium alloy on graphene oxide nanosheets with exceptional activity for electrochemical oxidation of ethanol. Mikrochimica Acta, 2014, 181, 373-380.	2.5	24
209	A stable and high resolution optical waveguide biosensor based on dense TiO 2 /Ag multilayer film. Applied Surface Science, 2016, 377, 207-212.	3.1	24
210	Unlocking the Electrocatalytic Activity of Chemically Inert Amorphous Carbonâ€Nitrogen for Oxygen Reduction: Discerning and Refactoring Chaotic Bonds. ChemElectroChem, 2017, 4, 1269-1273.	1.7	24
211	Magazineâ€Bendingâ€Inspired Architecting Antiâ€T of MXene Flakes with Vertical Ion Transport for Highâ€Performance Supercapacitors. Advanced Materials Interfaces, 2019, 6, 1900160.	1.9	24
212	In-plane Assembly of Distinctive 2D MOFs with Optimum Supercapacitive Performance. IScience, 2020, 23, 101220.	1.9	24
213	Etching-courtesy NH4+ pre-intercalation enables highly-efficient Li+ storage of MXenes via the renaissance of interlayer redox. Journal of Energy Chemistry, 2022, 72, 26-32.	7.1	24
214	Correlations between substrate bias, microstructure and surface morphology of tetrahedral amorphous carbon films. Vacuum, 2003, 72, 285-290.	1.6	23
215	The effects of electronic field on the atomic structure of the graphene/α-SiO2 interface. Nanotechnology, 2008, 19, 275710.	1.3	23
216	A growth mechanism for graphene deposited on polycrystalline Co film by plasma enhanced chemical vapor deposition. New Journal of Chemistry, 2013, 37, 1616.	1.4	23

#	Article	IF	CITATIONS
217	Nature of Tunable Optical Reflectivity of Rocksalt Hafnium Nitride Films. Journal of Physical Chemistry C, 2014, 118, 20511-20520.	1.5	23
218	Towards unlocking high-performance of supercapacitors: From layered transition-metal hydroxide electrode to redox electrolyte. Science China Technological Sciences, 2015, 58, 1779-1798.	2.0	23
219	Modulation of electronic properties from stacking orders and spin-orbit coupling for 3R-type MoS2. Scientific Reports, 2016, 6, 24140.	1.6	23
220	Supersaturation-controlled surface structure evolution of Pd@Pt core–shell nanocrystals: enhancement of the ORR activity at a sub-10 nm scale. Nanoscale, 2016, 8, 1698-1703.	2.8	23
221	Structural metatransition of energetically tangled crystalline phases. Physical Chemistry Chemical Physics, 2017, 19, 4560-4566.	1.3	23
222	Spectroscopic investigation on carbon nanotubes coated with ZnO nanoparticles. Journal Physics D: Applied Physics, 2008, 41, 065308.	1.3	22
223	Skin dominance of the dielectric–electronic–phononic–photonic attribute of nanoscaled silicon. Surface Science Reports, 2013, 68, 418-445.	3.8	22
224	Ice Regelation: Hydrogen-bond extraordinary recoverability and water quasisolid-phase-boundary dispersivity. Scientific Reports, 2015, 5, 13655.	1.6	22
225	Construction of a ternary hybrid of CdS nanoparticles loaded on mesoporous-TiO <sub>2</sub> /RGO for the enhancement of photocatalytic activity. RSC Advances, 2016, 6, 84722-84729.	1.7	22
226	Enhancement of oxidation resistance via a self-healing boron carbide coating on diamond particles. Scientific Reports, 2016, 6, 20198.	1.6	22
227	Plasmonic ZnO nanorods/Au substrates for protein microarrays with high sensitivity and broad dynamic range. Sensors and Actuators B: Chemical, 2016, 228, 231-236.	4.0	22
228	Dense Sm and Mn Co-Doped BaTiO3 Ceramics with High Permittivity. Materials, 2019, 12, 678.	1.3	22
229	Modulating Hardness in Molybdenum Monoborides by Adjusting an Array of Boron Zigzag Chains. Chemistry of Materials, 2019, 31, 200-206.	3.2	22
230	Thermoelectric properties of monolayer GeAsSe and SnSbTe. Journal of Materials Chemistry C, 2020, 8, 9763-9774.	2.7	22
231	Synthesis and characteristics of nanocrystalline Co/N thin film containing Co4N phase. Materials Science and Engineering B: Solid-State Materials for Advanced Technology, 2008, 150, 121-124.	1.7	21
232	Synthesis of graphene on a Ni film by radio-frequency plasma-enhanced chemical vapor deposition. Science Bulletin, 2012, 57, 3040-3044.	1.7	21
233	Synthesis of flower-shape palladium nanostructures on graphene oxide for electrocatalytic applications. Journal of Physics and Chemistry of Solids, 2013, 74, 1470-1474.	1.9	21
234	Density functional theory study of Li binding to graphene. RSC Advances, 2016, 6, 26540-26545.	1.7	21

Weitao Zheng

#	Article	IF	CITATIONS
235	Highly stable Au/Pd@mesoporous SiO <sub>2</sub> yolk–shell hetero-nanostructures for plasmon-enhanced visible light driven catalytic reactions. New Journal of Chemistry, 2017, 41, 786-792.	1.4	21
236	Increasing the range of non-noble-metal single-atom catalysts. Chinese Journal of Catalysis, 2017, 38, 1489-1497.	6.9	21
237	Accessible 3D Integrative Paper Electrode Shapes: Allâ€Carbon Dualâ€Ion Batteries with Optimum Packaging Performances. ChemElectroChem, 2017, 4, 3238-3243.	1.7	21
238	Nanocrystalline gold with small size: inverse Hall–Petch between mixed regime and super-soft regime. Philosophical Magazine, 2020, 100, 2335-2351.	0.7	21
239	Solution-processable carbon dots with efficient solid-state red/near-infrared emission. Journal of Colloid and Interface Science, 2022, 613, 547-553.	5.0	21
240	Effects of deposition parameters on microstructure of CrN/Si3N4 nanolayered coatings and their thermal stability. Journal of Physics Condensed Matter, 2005, 17, 6405-6413.	0.7	20
241	Size effects on the Kauzmann temperature and related thermodynamic parameters of Ag nanoparticles. Nanotechnology, 2007, 18, 255706.	1.3	20
242	Effects of modulation periodicity on microstructure, mechanical and tribological properties of NbN/AlN nanostructured multilayer films. Applied Surface Science, 2013, 284, 331-339.	3.1	20
243	Stability of Pt near surface alloys under electrochemical conditions: a model study. Physical Chemistry Chemical Physics, 2014, 16, 16615-16622.	1.3	20
244	Exsolutionâ€Mimic Heterogeneous Surfaces: Towards Unlimited Catalyst Design. ChemCatChem, 2015, 7, 48-50.	1.8	20
245	Understanding phase-change materials with unexpectedly low resistance drift for phase-change memories. Journal of Materials Chemistry C, 2018, 6, 3387-3394.	2.7	20
246	Passivation of the surface imperfection of TiO <sub>2</sub> by using ZIF-8 for efficient carrier separation/transfer. Dalton Transactions, 2018, 47, 209-214.	1.6	20
247	Storage of Na in layered graphdiyne as high capacity anode materials for sodium ion batteries. Journal of Materials Chemistry A, 2019, 7, 25609-25618.	5.2	20
248	Polymeric Nanoâ€Blueâ€Energy Generator Based on Anionâ€Selective Ionomers with 3D Pores and pHâ€Driving Gating. Advanced Energy Materials, 2020, 10, 2001552.	10.2	20
249	Diffusionless‣ike Transformation Unlocks Pseudocapacitance with Bulk Utilization: Reinventing Fe <sub>2</sub> O <sub>3</sub> in Alkaline Electrolyte. Energy and Environmental Materials, 2023, 6, .	7.3	20
250	Crystallization behaviors of secondarily quenched Nylon 6. Materials Letters, 2007, 61, 925-928.	1.3	19
251	Finite-Size Effect on Band Structure and Photoluminescence of Semiconductor Nanocrystals. IEEE Nanotechnology Magazine, 2008, 7, 5-9.	1.1	19
252	Relatively low temperature synthesis of hexagonal tungsten carbide films by N doping and its effect on the preferred orientation, phase transition, and mechanical properties. Journal of Vacuum Science and Technology A: Vacuum, Surfaces and Films, 2009, 27, 167-173.	0.9	19

#	Article	IF	CITATIONS
253	Visible photocatalytic activity enhancement of Zn0.8Cd0.2S by hybridization of reduced graphene oxide. Materials Letters, 2013, 109, 100-103.	1.3	19
254	In situ preparation of porous Pd nanotubes on a GCE for non-enzymatic electrochemical glucose sensors. Analytical Methods, 2015, 7, 8605-8610.	1.3	19
255	Morphology dependence of electrochemical properties on palladium nanocrystals. Journal of Colloid and Interface Science, 2017, 490, 190-196.	5.0	19
256	Magnetron Sputtering Deposition Cu@Onion-like N–C as High-Performance Electrocatalysts for Oxygen Reduction Reaction. ACS Applied Materials & Interfaces, 2017, 9, 41945-41954.	4.0	19
257	Ultralow-Friction and Ultralow-Wear TiN-Ag Solid Solution Coating in Base Oil. Journal of Physical Chemistry Letters, 2020, 11, 1614-1621.	2.1	19
258	Increasing sp3hybridized carbon atoms in germanium carbide films by increasing the argon ion energy and germanium content. Journal Physics D: Applied Physics, 2010, 43, 135103.	1.3	18
259	Hydrogen adsorption on Ce/SWCNT systems: a DFT study. Physical Chemistry Chemical Physics, 2011, 13, 9483.	1.3	18
260	Frequency response of graphene phonons to heating and compression. Applied Physics Letters, 2011, 99, 133108.	1.5	18
261	Synthesis of Novel Hollow ZnSnO <sub>3</sub> Cubic Nanocages and Their HCHO Sensing Properties. Journal of Nanoscience and Nanotechnology, 2013, 13, 1286-1290.	0.9	18
262	Investigating the interaction of dye molecules with graphene oxide by using a surface plasmon resonance technique. RSC Advances, 2014, 4, 50789-50794.	1.7	18
263	TM atoms on B/N doped defective graphene as a catalyst for oxygen reduction reaction: a theoretical study. RSC Advances, 2015, 5, 82804-82812.	1.7	18
264	Electrochemical modeling and parameter identification based on bacterial foraging optimization algorithm for lithium-ion batteries. Journal of Applied Electrochemistry, 2016, 46, 1119-1131.	1.5	18
265	Development of novel and ultrahigh-performance asymmetric supercapacitor based on redox electrode-electrolyte system. Electrochimica Acta, 2017, 231, 495-501.	2.6	18
266	Facile band alignment of C3N4/CdS/MoS2 sandwich hybrid for efficient charge separation and high photochemical performance under visible-light. Powder Technology, 2019, 351, 222-228.	2.1	18
267	High-density/efficient surface active sites on modified separators to boost Li-S batteries via atomic Co3+-Se termination. Nano Research, 2022, 15, 7199-7208.	5.8	18
268	Effects of radio frequency power on the chemical bonding, optical and mechanical properties for radio frequency reactive sputtered germanium carbide films. Journal Physics D: Applied Physics, 2006, 39, 5074-5079.	1.3	17
269	Synthesis and field electron emission properties of hybrid carbon nanotubes and nanoparticles. Nanotechnology, 2008, 19, 065710.	1.3	17
270	Simple and eco-friendly solvothermal synthesis of luminescent reduced graphene oxide small sheets. Materials Letters, 2012, 78, 170-173.	1.3	17

#	Article	IF	CITATIONS
271	R6G molecule induced modulation of the optical properties of reduced graphene oxide nanosheets for use in ultrasensitive SPR sensing. Scientific Reports, 2016, 6, 21254.	1.6	17
272	Sn(II)-Containing Phosphates as Optoelectronic Materials. Chemistry of Materials, 2017, 29, 2459-2465.	3.2	17
273	Activating an MXene as a host for EMIm <sup>+</sup> by electrochemistry-driven Fe-ion pre-intercalation. Journal of Materials Chemistry A, 2020, 8, 16265-16270.	5.2	17
274	Improved thermoelectric transport properties of Ge <sub>4</sub> Se <sub>3</sub> Te through dimensionality reduction. Journal of Materials Chemistry C, 2021, 9, 1804-1813.	2.7	17
275	Boosting the kinetics of PF6â^' into graphitic layers for the optimal cathode of dual-ion batteries: The rehearsal of pre-intercalating Li+. Journal of Energy Chemistry, 2022, 71, 392-399.	7.1	17
276	Behaviors of Monomer H <sub>2</sub> O on the Cu(111) Surface under Surface Charges. Journal of Physical Chemistry C, 2010, 114, 19331-19337.	1.5	16
277	High-speed creep process mediated by rapid dislocation absorption in nanocrystalline Cu. Journal of Applied Physics, 2012, 111, 063506.	1.1	16
278	Crystal and electronic structures of superhard B2CN : An ab initio study. Solid State Communications, 2012, 152, 71-75.	0.9	16
279	Fundamental insights into the electronic structure of zigzag MoS <sub>2</sub> nanoribbons. Physical Chemistry Chemical Physics, 2016, 18, 4675-4683.	1.3	16
280	Compressed few-layer black phosphorus nanosheets from semiconducting to metallic transition with the highest symmetry. Nanoscale, 2017, 9, 10741-10749.	2.8	16
281	Improving frictional properties of DLC films by surface energy manipulation. RSC Advances, 2018, 8, 11388-11394.	1.7	16
282	Incorporating a Polar Molecule to Passivate Defects for Perovskite Solar Cells. Solar Rrl, 2020, 4, 1900489.	3.1	16
283	First-Principles Calculation of Optimizing the Performance of Germanene-Based Supercapacitors by Vacancies and Metal Atoms. Journal of Physical Chemistry C, 2020, 124, 12346-12358.	1.5	16
284	Methanol-induced fast CsBr release results in phase-pure CsPbBr <sub>3</sub> perovskite nanoplatelets. Nanoscale Advances, 2020, 2, 1973-1979.	2.2	16
285	Electron Delocalization in CsPbI <sub>3</sub> Quantum Dots Enables Efficient Lightâ€Emitting Diodes with Improved Efficiency Rollâ€Off. Advanced Optical Materials, 2022, 10, .	3.6	16
286	Field-Emission Mechanism of Island-Shaped Graphene–BN Nanocomposite. Journal of Physical Chemistry C, 2011, 115, 9471-9476.	1.5	15
287	Number-of-layer discriminated graphene phonon softening and stiffening. Applied Physics Letters, 2011, 99, 163109.	1.5	15
288	XPS quantification of the hetero-junction interface energy. Applied Surface Science, 2013, 265, 71-77.	3.1	15

#	Article	IF	CITATIONS
289	Highly hard yet toughened bcc-W coating by doping unexpectedly low B content. Scientific Reports, 2017, 7, 9353.	1.6	15
290	Strain-induced modulations of electronic structure and electron–phonon coupling in dense H <sub>3</sub> S. Physical Chemistry Chemical Physics, 2018, 20, 5952-5957.	1.3	15
291	2D Bismuthene Metal Electron Mediator Engineering Super Interfacial Charge Transfer for Efficient Photocatalytic Reduction of Carbon Dioxide. ACS Applied Materials & Interfaces, 2021, 13, 21582-21592.	4.0	15
292	Raman spectroscopy and correlativeâ€Raman technology excel as an optimal stage for carbonâ€based electrode materials in electrochemical energy storage. Journal of Raman Spectroscopy, 2021, 52, 2119-2130.	1.2	15
293	Oxygenation mediating the valence density-of-states and work function of Ti(0001) skin. Physical Chemistry Chemical Physics, 2015, 17, 9867-9872.	1.3	14
294	Lithiation and Sodiation of Hydrogenated Silicene: A Density Functional Theory Investigation. ChemSusChem, 2021, 14, 5460-5469.	3.6	14
295	Improved One- and Multiple-Photon Excited Photoluminescence from Cd2+-Doped CsPbBr3 Perovskite NCs. Nanomaterials, 2022, 12, 151.	1.9	14
296	Light-emitting boron nitride nanoparticles encapsulated in zeolite ZSM-5. Microporous and Mesoporous Materials, 2000, 40, 263-269.	2.2	13
297	Blue photoluminescence from SiC nanoparticles encapsulated in ZSM-5. Materials Letters, 2001, 48, 242-246.	1.3	13
298	Distinct Young's modulus of nanostructured materials in comparison with nanocrystals. Physical Chemistry Chemical Physics, 2011, 13, 21328.	1.3	13
299	Interaction of Rhodamine 6G molecules with graphene: a combined computational–experimental study. Physical Chemistry Chemical Physics, 2016, 18, 28418-28427.	1.3	13
300	Theoretical study of electronic and mechanical properties of Fe <sub>2</sub> B. RSC Advances, 2016, 6, 73576-73580.	1.7	13
301	Pinpointing single metal atom anchoring sites in carbon for oxygen reduction: Doping sites or defects?. Chinese Journal of Catalysis, 2018, 39, 4-7.	6.9	13
302	Influence of oxygen on the growth of carbon nanotubes. Journal Physics D: Applied Physics, 2008, 41, 205306.	1.3	12
303	Modulation periodicity dependent structure, stress, and hardness in NbN/W2N nanostructured multilayer films. Journal of Applied Physics, 2011, 109, .	1.1	12
304	Role of carbon in the formation of hard Ge1â^'xCx thin films by reactive magnetron sputtering. Physica B: Condensed Matter, 2011, 406, 2658-2662.	1.3	12
305	One-step synthesis of N-doped amorphous carbon at relatively low temperature as excellent metal-free electrocatalyst for oxygen reduction. Catalysis Communications, 2014, 46, 161-164.	1.6	12
306	Structural, mechanical properties and fracture mechanism of RuB1.1. Dalton Transactions, 2014, 43, 5168.	1.6	12

#	Article	IF	CITATIONS
307	Magnetism in Na-filled Fe-based skutterudites. Scientific Reports, 2015, 5, 10782.	1.6	12
308	The role of trace Fe in Fe–N-doped amorphous carbon with excellent electrocatalytic performance for oxygen reduction reaction. Catalysis Communications, 2015, 60, 37-41.	1.6	12
309	Photochemical growth of silver nanoparticles with mixed-light irradiation. Colloid and Polymer Science, 2016, 294, 911-916.	1.0	12
310	Synthesis and characterization of noble metal borides: RuB (x> 1). Materials Research Bulletin, 2016, 74, 188-191.	2.7	12
311	Improving electrical conductivity and wear resistance of hafnium nitride films via tantalum incorporation. Ceramics International, 2017, 43, 8517-8524.	2.3	12
312	Localized inside-out Ostwald ripening of hybrid double-shelled cages into SnO <sub>2</sub> triple-shelled hollow cubes for improved toluene detection. Nanoscale, 2020, 12, 2011-2021.	2.8	12
313	Enhancing the Efficiency and Stability of CsPbl <sub>3</sub> Nanocrystal-Based Light-Emitting Diodes through Ligand Engineering with Octylamine. Journal of Physical Chemistry C, 2022, 126, 1085-1093.	1.5	12
314	Comment on "Correlation of x-ray absorption and x-ray photoemission spectroscopies in amorphous carbon nitride― Physical Review B, 2001, 64, .	1.1	11
315	Amorphous hollow carbon spheres synthesized using radio frequency plasma-enhanced chemical vapour deposition. Journal Physics D: Applied Physics, 2008, 41, 195504.	1.3	11
316	Stabilization of Pt monolayer catalysts under harsh conditions of fuel cells. Journal of Chemical Physics, 2015, 142, 194710.	1.2	11
317	TiO2 Band Restructuring by B and P Dopants. PLoS ONE, 2016, 11, e0152726.	1.1	11
318	Modulation of the shape and localized surface plasmon resonance of silver nanoparticles via halide ion etching and photochemical regrowth. Materials Letters, 2016, 173, 88-90.	1.3	11
319	Structural instability and magnetism of superconducting <mml:math xmlns:mml="http://www.w3.org/1998/Math/MathML"&gt; <mml:mrow> <mml:msub> <mml:mi>KCr</mml:mi> <mml: Physical Review B, 2019, 99, .</mml: </mml:msub></mml:mrow></mml:math 	mnıxB <td>ml±mn&gt;</td>	ml±mn>
320	Dual-Phase Nanocomposite TiB <sub>2</sub> /MoS <sub>1.7</sub> B <sub>0.3</sub> : An Excellent Ultralow Friction and Ultralow Wear Self-Lubricating Material. ACS Applied Materials & Interfaces, 2021, 13, 59352-59363.	4.0	11
321	Electron spin resonance analysis of magnetic structures in La2/3Ca1/3MnO3. Journal of Magnetism and Magnetic Materials, 2005, 293, 782-786.	1.0	10
322	Relationship between dielectric coefficient and Urbach tail width of hydrogenated amorphous germanium carbon alloy films. Applied Physics Letters, 2012, 101, 042109.	1.5	10
323	Correlation between interfacial electronic structure and mechanical properties of ZrN/SiNx films. Materials Letters, 2013, 94, 61-64.	1.3	10
324	Free-Standing Single-Molecule Thick Crystals Consisting of Linear Long-Chain Polymers. Nano Letters, 2017, 17, 1655-1659.	4.5	10

#	Article	IF	CITATIONS
325	Color-Stable and High-Efficiency Blue Perovskite Nanocrystal Light-Emitting Diodes via Monovalent Copper Ion Lowering Lead Defects. ACS Applied Materials & Interfaces, 2021, 13, 55380-55390.	4.0	10
326	Surface morphology and dynamic scaling in growth of iron nitride thin films deposited by dc magnetron sputtering. Journal of Vacuum Science and Technology A: Vacuum, Surfaces and Films, 2003, 21, 983-987.	0.9	9
327	Two types of carbon nanocomposites: Graphite encapsulated iron nanoparticles and thin carbon nanotubes supported on thick carbon nanotubes, synthesized using PECVD. Journal of Solid State Chemistry, 2009, 182, 966-972.	1.4	9
328	ULTRAFINE AU NANODOTS ON GRAPHENE OXIDE FOR CATALYTIC REDUCTION OF 4-NITROPHENOL. Nano, 2013, 08, 1350034.	0.5	9
329	Phase stability, hardness and bond characteristics of ruthenium borides from first-principles. RSC Advances, 2014, 4, 25093-25098.	1.7	9
330	Adsorption and diffusion of Li with S on pristine and defected graphene. Physical Chemistry Chemical Physics, 2016, 18, 31268-31276.	1.3	9
331	Sn2Se3: A conducting crystalline mixed valent phase change memory compound. Journal of Applied Physics, 2017, 121, .	1.1	9
332	Rationalizing the Anion Storage in Cathodes for Optimum Dual-Ion Batteries: State of the Art and the Prospect. Energy & Fuels, 2020, 34, 15701-15713.	2.5	9
333	BN and Si nanostructures: preparation and visible photoluminescence properties. Materials Letters, 2000, 44, 341-346.	1.3	8
334	Unusual Crystallization Behavior in Nylon-6 and Nylon-6/Montmorillonite Nanocomposite Films. Macromolecular Rapid Communications, 2004, 25, 1340-1344.	2.0	8
335	Grain-size effect on the preferred orientation of TiC/α-C:H thin films. Applied Surface Science, 2012, 258, 6800-6806.	3.1	8
336	First-principle calculations on the structural stability and electronic properties of superhard B <sub><i>x</i></sub> C <sub><i>y</i></sub> compounds. Journal of Physics Condensed Matter, 2013, 25, 425502.	0.7	8
337	Optical reflectivity and hardness improvement of hafnium nitride films via tantalum alloying. Applied Physics Letters, 2016, 109, 232102.	1.5	8
338	Supercapacitors: Inverted Design for Highâ€Performance Supercapacitor Via Co(OH) <sub>2</sub> â€Derived Highly Oriented MOF Electrodes (Adv. Energy Mater. 7/2018). Advanced Energy Materials, 2018, 8, 1870030.	10.2	8
339	Interface engineered surface morphology evolution of Au@Pd core–shell nanorods. Nanoscale, 2018, 10, 21161-21167.	2.8	8
340	Self-crystallized Interlayer Integrating Polysulfide-adsorbed TiO2/TiO and Highly-electron-conductive TiO for High-stability Lithium-sulfur Batteries. Chemical Research in Chinese Universities, 2021, 37, 259-264.	1.3	8
341	Unlocking the potential of metal organic frameworks for synergized specific and areal capacitances via orientation regulation. Nanotechnology, 2021, 32, 075402.	1.3	8
342	Macroscale Robust Superlubricity on Metallic NbB <sub>2</sub> . Advanced Science, 2022, 9, e2103815.	5.6	8

#	Article	IF	CITATIONS
343	Photo-less catalysis of TiO2-reduced graphene oxides. Chemical Physics Letters, 2014, 608, 229-234.	1.2	7
344	First-principles investigations on the adsorption and diffusion of carbon atoms on the surface and in the subsurface of Co (111) related to the growth of graphene. RSC Advances, 2014, 4, 34237.	1.7	7
345	Electronic and magnetic properties of nitrogen-doped graphene nanoribbons with grain boundary. RSC Advances, 2014, 4, 1503-1511.	1.7	7
346	Transformation of electronic properties and structural phase transition from HfN to Hf <sub>3</sub> N <sub>4</sub> . Journal of Physics Condensed Matter, 2015, 27, 225501.	0.7	7
347	One-Pot Synthesis of Nanodendritic PtIr Alloy with High Electrochemical Activity for Ethylene Glycol Oxidation. Nano, 2017, 12, 1750026.	0.5	7
348	A universal strategy to improve interfacial kinetics of solid supercapacitors used in high temperature. Journal of Colloid and Interface Science, 2021, 586, 110-119.	5.0	7
349	<i>In situ</i> growth of ultra-smooth or super-rough thin films by suppression of vertical or horizontal growth of surface mounds. Journal of Materials Chemistry C, 2020, 8, 3248-3257.	2.7	7
350	Superhard metallic compound <mml:math xmlns:mml="http://www.w3.org/1998/Math/MathML"&gt;<mml:msub><mml:mi>TaB</mml:mi><mml:mn>2via crystal orientation resolved strain stiffening. Physical Review B, 2022, 105, .</mml:mn></mml:msub></mml:math 	mn <b>p.1</b> /mm	l:msub>
351	Investigation on Nanodiamond and Carbon Nanotubeâ€Diamond Nanocomposite Synthesized using RFâ€PECVD. Chemical Vapor Deposition, 2008, 14, 236-240.	1.4	6
352	First-principles calculations on the structure and electronic properties of boron doping zigzag single-walled carbon nanotubes. Science in China Series D: Earth Sciences, 2009, 52, 1219-1224.	0.9	6
353	Controllable fabrication of carbon nanotubes on catalysts derived from PS-b-P2VP block copolymer template and in situ synthesis of carbon nanotubes/Au nanoparticles composite materials. Materials Chemistry and Physics, 2010, 119, 249-253.	2.0	6
354	Purified rhodium edge states: undercoordination-induced quantum entrapment and polarization. Physical Chemistry Chemical Physics, 2010, 12, 12494.	1.3	6
355	Atomic Scale Purification of Re Surface Kink States with and without Oxygen Chemisorption. Journal of Physical Chemistry C, 2011, 115, 7450-7455.	1.5	6
356	Synthesis and characterization of amorphous hollow carbon spheres. Journal of Materials Science, 2012, 47, 2072-2077.	1.7	6
357	A simple method to synthesize graphitic mesoporous carbon materials with different structures. Journal of Porous Materials, 2013, 20, 983-988.	1.3	6
358	How important is the {103} plane of stable Ge <sub>2</sub> Sb <sub>2</sub> Te <sub>5</sub> for phase hange memory?. Journal of Microscopy, 2015, 259, 10-15.	0.8	6
359	Near infrared electroluminescence of ZnMgO/InN core–shell nanorod heterostructures grown on Si substrate. Physical Chemistry Chemical Physics, 2016, 18, 20812-20818.	1.3	6
360	Evolution of Water Structures on Stepped Platinum Surfaces. Journal of Physical Chemistry C, 2018, 122, 604-611.	1.5	6

#	Article	IF	CITATIONS
361	Designing chemical bonds between active materials and current collectors for packaging a high-performance supercapacitor. Nanotechnology, 2020, 31, 105402.	1.3	6
362	Adsorption of K Ions on Single-Layer GeC for Potential Anode of K Ion Batteries. Nanomaterials, 2021, 11, 1900.	1.9	6
363	Interior Melting of Rapidly Heated Gold Nanoparticles. Journal of Physical Chemistry Letters, 2021, 12, 8170-8177.	2.1	6
364	The universality classes in growth of iron nitride thin films deposited by magnetron sputtering. Materials Chemistry and Physics, 2003, 82, 254-257.	2.0	5
365	Flow stress of Ni-rich NiTi thin films. Journal of Materials Science, 2005, 40, 537-538.	1.7	5
366	Dynamic Isomer Shift in Charge-Ordering Manganite Y0.5Ca0.5MnO3: Mössbauer Spectroscopy Study. Journal of Physical Chemistry B, 2005, 109, 1656-1659.	1.2	5
367	High pressure synthesis and characterization of noble metal nitride IrNx. Materials Letters, 2013, 107, 382-385.	1.3	5
368	Catalytic nature of under- and hetero-coordinated atoms resolved using zone-selective photoelectron spectroscopy (ZPS). Vacuum, 2014, 100, 87-91.	1.6	5
369	Hardness and optical gap enhancement of germanium carbon films by nitrogen incorporation. Thin Solid Films, 2015, 584, 208-213.	0.8	5
370	Enhanced cycling stability of Ni-MH battery by depositing amorphous carbon film on the Ti1.4V0.6Ni negative electrode. Diamond and Related Materials, 2016, 66, 10-15.	1.8	5
371	Synthesis of Silver Nanoprisms and Nanodecahedra for Plasmonic Modulating Surface-Enhanced Raman Scattering. Journal of Nanoscience and Nanotechnology, 2016, 16, 6829-6836.	0.9	5
372	Ultrathin Carbon Film Protected Silver Nanostructures for Surface-Enhanced Raman Scattering. Applied Spectroscopy, 2016, 70, 1751-1758.	1.2	5
373	Breaking the lithium storage limit via independent bilayer units within 2D layer materials. Journal of Energy Chemistry, 2020, 41, 1-2.	7.1	5
374	Deformation and ductile fracture of nanocrystalline gold ultrathin nanoribbon: Width effect. Fatigue and Fracture of Engineering Materials and Structures, 2021, 44, 1850-1861.	1.7	5
375	Structure and properties of carbon nitride films deposited by magnetron sputtering. Materials Chemistry and Physics, 1999, 60, 163-167.	2.0	4
376	The Effect of Substrate Temperature on the Structure and Hardness of Magnetron Sputtering Deposited Carbon Nitride Films. Physica Status Solidi A, 1999, 172, 373-378.	1.7	4
377	Field electron emission enhancement of amorphous carbon through a niobium buffer layer. Journal of Applied Physics, 2008, 103, 114314.	1.1	4
378	Small angle X-ray scattering study of the strengthen mechanism of Al–Mg–Li alloy during retrogression and reaging treatment. Journal of Alloys and Compounds, 2010, 503, 291-293.	2.8	4

#	Article	IF	CITATIONS
379	Controllable synthesis of a novel hedgehog-like core/shell structure. Journal of Solid State Chemistry, 2012, 186, 235-239.	1.4	4
380	Confinement of massless Dirac fermions in the graphene matrix induced by the B/N heteroatoms. Physical Chemistry Chemical Physics, 2015, 17, 5586-5593.	1.3	4
381	Melting of Nanocrystalline Gold. Journal of Physical Chemistry C, 2019, 123, 907-914.	1.5	4
382	Storage mechanism of K in hydrogen-substituted graphdiyne as a superior anode. Journal of Materials Chemistry A, 2021, 9, 12320-12330.	5.2	4
383	Progress of graphdiyne-based materials for anodes of alkali metal ion batteries. Nano Futures, 2022, 6, 022004.	1.0	4
384	The change of Morin transition temperature in nanocrystalline α-Fe2O3. Science Bulletin, 1997, 42, 344-346.	1.7	3
385	<i>AB INITIO</i> STUDY OF NITROGEN-DOPED CARBON NANOTUBES. Nano, 2007, 02, 181-188.	0.5	3
386	Enhanced Field Electron Emission Properties of Hybrid Carbon Nanotubes Synthesized by RFâ€₽ECVD. Chemical Vapor Deposition, 2009, 15, 291-295.	1.4	3
387	Investigation on Mechanical Properties of Deformation TiNi Thin Films. Journal of Materials Engineering and Performance, 2012, 21, 2691-2694.	1.2	3
388	Gap openings in graphene regarding interfacial interaction from substrates. Physical Chemistry Chemical Physics, 2014, 16, 5600.	1.3	3
389	Pressure evolution of the potential barriers for transformations of layered BN to dense structures. RSC Advances, 2015, 5, 87550-87555.	1.7	3
390	Ion-bombardment-induced reduction in vacancies and its enhanced effect on conductivity and reflectivity in hafnium nitride films. Applied Physics A: Materials Science and Processing, 2016, 122, 1.	1.1	3
391	Surface roughening transition induced by phase transformation in hafnium nitride films. Surface and Coatings Technology, 2017, 320, 414-420.	2.2	3
392	The Effect of Strain Rate on the Deformation Processes of NC Gold with Small Grain Size. Crystals, 2020, 10, 858.	1.0	3
393	Correlation between structure and hardness of magnetron sputtering deposited CNx films. Science Bulletin, 1999, 44, 1149-1152.	1.7	2
394	CRYSTALLINE CARBON NITRIDE FILMS GROWN BY MICROWAVE PLASMA CHEMICAL VAPOR DEPOSITION. International Journal of Modern Physics B, 2002, 16, 1091-1095.	1.0	2
395	The effects of Si3N4 interlayer on the thermal stability and hardness of Ti/TiNx (x=0.5–1) nanolayered coatings. Applied Surface Science, 2007, 253, 7238-7241.	3.1	2
396	Field electron emission enhancement of amorphous carbon through a niobium carbide buffer layer. Journal of Applied Physics, 2009, 105, .	1.1	2

#	Article	IF	CITATIONS
397	Patterned Carbon Nanotubes Fabricated by the Combination of Microcontact Printing and Diblock Copolymer Micelles. Journal of Nanoscience and Nanotechnology, 2010, 10, 508-513.	0.9	2
398	Exploration of Defect Structures on Graphene. Journal of Nanoscience and Nanotechnology, 2013, 13, 1030-1034.	0.9	2
399	Electronâ€Irradiationâ€Stimulated Atomicâ€Scale Structural Dynamics of the Pentagonal Channel in a Complex MoVTeNbO <sub><i>x</i></sub> Catalyst. ChemCatChem, 2015, 7, 3651-3654.	1.8	2
400	Toward structural/chemical cotailoring of phaseâ€change Ge–Sb–Te in a transmission electron microscope. Journal of Microscopy, 2015, 257, 253-255.	0.8	2
401	Structural evolution and optical properties of hydrogenated germanium carbonitride films. Vacuum, 2016, 129, 23-30.	1.6	2
402	Highly oriented lamellar polyaniline films via electrochemical polymerization and post-growth annealing. RSC Advances, 2017, 7, 3819-3822.	1.7	2
403	Combined effect of ion bombardment and nitrogen incorporation on structure, mechanical and optical properties of amorphous Ge2Sb2Te5 films. Vacuum, 2017, 141, 32-40.	1.6	2
404	Robust Synthesis of Highâ€Performance Nâ€Graphite Hollow Nanocatalysts Based on the Ostwald Ripening Mechanism for Oxygen Reduction Reaction Electrocatalysis. Particle and Particle Systems Characterization, 2018, 35, 1800266.	1.2	2
405	Photoluminescence: Thermally Activated Upconversion Nearâ€Infrared Photoluminescence from Carbon Dots Synthesized via Microwave Assisted Exfoliation (Small 50/2019). Small, 2019, 15, 1970288.	5.2	2
406	Full-color, multi-level transmittance modulators: From reflectivity/gradient absorption coupling mechanism to materials map. Acta Materialia, 2021, 216, 117132.	3.8	2
407	A dual-control strategy based on electrode material and electrolyte optimization to construct an asymmetric supercapacitor with high energy density. Nanotechnology, 2022, , .	1.3	2
408	Synergetic interfacial passivation, band alignment, and long-term stability with halide-optimized CsPbBr <sub><i>x</i></sub> l <sub>3â^`<i>x</i></sub> nanocrystals for high-efficiency MAPbl <sub>3</sub> solar cells. Journal of Materials Chemistry C, 2022, 10, 5134-5140.	2.7	2
409	X-ray reflectivity and diffraction investigation on TiN/SiNx nanolayered coatings deposited by magnetron sputtering. Powder Diffraction, 2007, 22, 316-318.	0.4	1
410	Effects of bonding structure from niobium carbide buffer layer on the field electric emission properties of a-C films. Journal of Applied Physics, 2009, 105, 074318.	1.1	1
411	Preparation and Application of Noble Metallic Plasmonic Nanostructures. , 2015, , .		1
412	Vertical Ion Transport: Magazineâ€Bendingâ€Inspired Architecting Antiâ€T of MXene Flakes with Vertical Ion Transport for Highâ€Performance Supercapacitors (Adv. Mater. Interfaces 8/2019). Advanced Materials Interfaces, 2019, 6, 1970051.	1.9	1
413	Designing infrared phase change materials for colorful infrared transmittance modulators. Applied Surface Science, 2022, 600, 154104.	3.1	1
414	Theoretical Temperatureâ€Pressure Curves for Cu, Ag, and Au at High Melting. Physica Status Solidi (B): Basic Research, 1991, 168, K5.	0.7	0

#	Article	IF	CITATIONS
415	Dynamic Isomer Shift in Charge-Ordering Manganite Y0.5Ca0.5MnO3: Moessbauer Spectroscopy Study ChemInform, 2005, 36, no.	0.1	0
416	The enhanced nucleation factors and field electron emission property of diamond synthesized by RF-PECVD. Journal of Alloys and Compounds, 2012, 517, 98-102.	2.8	0
417	Single Atoms: Single Atom Excels as the Smallest Functional Material (Adv. Funct. Mater. 18/2016). Advanced Functional Materials, 2016, 26, 2987-2987.	7.8	0
418	Blue Energy: Polymeric Nanoâ€Blueâ€Energy Generator Based on Anionâ€5elective Ionomers with 3D Pores and pHâ€Driving Gating (Adv. Energy Mater. 44/2020). Advanced Energy Materials, 2020, 10, 2070182.	10.2	0
419	30.3: Invited Paper: CsPbX 3 perovskite highâ€definition display materials and LEDs. Digest of Technical Papers SID International Symposium, 2021, 52, 409-409.	0.1	0
420	Microhardness and Deformation Storage Energy Density of NiTi Thin Films. , 2013, , 1959-1966.		0
421	Microhardness and Deformation Storage Energy Density of NiTi Thin Films. , 2015, , 571-578.		0

Favorable Energy Band Alignment of TiO<sub>2</sub> Anatase/Rutile Heterophase Homojunctions Yields Photocatalytic Hydrogen Evolution with Quantum Efficiency Exceeding 45.6% (Adv. Energy) Tj ETQq0 0 0 rgB0,Dverlook 10 Tf 50 422